



Article

# Synthesis of Small Ce<sup>3+</sup>-Er<sup>3+</sup>-Yb<sup>3+</sup> Tri-Doped BaLuF<sub>5</sub> Active-Core-Active-Shell-Active-Shell Nanoparticles with Strong Down Conversion Luminescence at 1.5 μm

Yongling Zhang <sup>1,\*</sup> , Yudi Shi <sup>1</sup>, Zhengkun Qin <sup>1,\*</sup>, Mingxing Song <sup>1,\*</sup> and Weiping Qin <sup>2</sup><sup>1</sup> College of Information & Technology, Jilin Normal University, Siping 136000, China; shiyudijlu@163.com<sup>2</sup> State Key Laboratory on Integrated Optoelectronics, College of Electronic Science & Engineering, Jilin University, Changchun 130012, China; wpqin@jlu.edu.cn

\* Correspondence: yonglling@163.com (Y.Z.); qin\_zhengkun@126.com (Z.Q.); mxsong@jlnu.edu.cn (M.S.); Tel.: +86-434-3292-050 (Y.Z. &amp; Z.Q. &amp; M.S.)

Received: 9 July 2018; Accepted: 3 August 2018; Published: 14 August 2018



**Abstract:** Small fluoride nanoparticles (NPs) with strong down-conversion (DC) luminescence at 1.5 μm are quite desirable for optical fiber communication systems. Nevertheless, a problem exists regarding how to synthesize small fluoride NPs with strong DC emission at 1.5 μm. Herein, we propose an approach to improve 1.5 μm emission of BaLuF<sub>5</sub>:Yb<sup>3+</sup>,Er<sup>3+</sup> NPs by way of combining doping Ce<sup>3+</sup> ions and coating multiple BaLuF<sub>5</sub>:Yb<sup>3+</sup> active-shells. We prepared the BaLuF<sub>5</sub>:18%Yb<sup>3+</sup>,2%Er<sup>3+</sup>,2%Ce<sup>3+</sup> NPs through a high-boiling solvent method. The effect of Ce<sup>3+</sup> concentration on the DC luminescence was systematically investigated in the BaLuF<sub>5</sub>:Yb<sup>3+</sup>,Er<sup>3+</sup> NPs. Under a 980 nm laser excitation, the intensities of 1.53 μm emission of BaLuF<sub>5</sub>:18%Yb<sup>3+</sup>,2%Er<sup>3+</sup>,2%Ce<sup>3+</sup> NPs was enhanced by 2.6 times comparing to that of BaLuF<sub>5</sub>:18%Yb<sup>3+</sup>,2%Er<sup>3+</sup> NPs since the energy transfer between Er<sup>3+</sup> and Ce<sup>3+</sup> ions: Er<sup>3+</sup>:<sup>4</sup>I<sub>11/2</sub> (Er<sup>3+</sup>) + <sup>2</sup>F<sub>5/2</sub> (Ce<sup>3+</sup>) → <sup>4</sup>I<sub>13/2</sub> (Er<sup>3+</sup>) + <sup>2</sup>F<sub>7/2</sub> (Ce<sup>3+</sup>). Then, we synthesized BaLuF<sub>5</sub>:18%Yb<sup>3+</sup>,2%Er<sup>3+</sup>,2%Ce<sup>3+</sup>@BaLuF<sub>5</sub>:5%Yb<sup>3+</sup>@BaLuF<sub>5</sub>:5%Yb<sup>3+</sup> core-active-shell-active-shell NPs via a layer-by-layer strategy. After coating two BaLuF<sub>5</sub>:Yb<sup>3+</sup> active-shell around BaLuF<sub>5</sub>:Yb<sup>3+</sup>,Er<sup>3+</sup>,Ce<sup>3+</sup> NPs, the intensities of the 1.53 μm emission was enhanced by 44 times compared to that of BaLuF<sub>5</sub>:Yb<sup>3+</sup>,Er<sup>3+</sup> core NPs, since the active-shells could be used to not only suppress surface quenching but also to transfer the pump light to the core region efficiently through Yb<sup>3+</sup> ions inside the active-shells.

**Keywords:** BaLuF<sub>5</sub>; nanoparticles; active-shell; core-shell; down conversion luminescence; 1.5 μm

## 1. Introduction

Recently, trivalent rare-earth (RE<sup>3+</sup>) ions doped fluoride nanoparticles (NPs) have been applied widely in many fields of high technology, such as bioimaging, drug delivery, photodynamic therapy, solar cells [1–12], etc. In particular, Er<sup>3+</sup>-doped fluoride NPs have been applied in waveguide amplifiers [13–16] since intra-4f-shell transitions of Er<sup>3+</sup> ions not only cause visible light emissions but also send an emission at 1.5 μm (the <sup>4</sup>I<sub>13/2</sub> → <sup>4</sup>I<sub>15/2</sub> transition of Er<sup>3+</sup> ions), which is located in low loss windows of optical communication networks. In order to get high-gain Er<sup>3+</sup>-doped waveguide amplifiers, Er<sup>3+</sup>-doped fluoride NPs should not only have a strong down-conversion luminescence at 1.5 μm, but also have a small size. So far, various strategies have been developed to improve luminescence intensity of Er<sup>3+</sup>-doped fluoride NPs at 1.5 μm. One is to increase the nonradiative decay rate that the high energy levels of Er<sup>3+</sup> ions relax nonradiatively to the <sup>4</sup>I<sub>13/2</sub> level [17–19]. Zhai et al.

synthesized  $\text{NaYF}_4:\text{Er}^{3+}, \text{Yb}^{3+}, \text{Ce}^{3+}$  NPs, and found the 1.53  $\mu\text{m}$  emission band of  $\text{Er}^{3+}$  ions in the NPs was enhanced by 6 times after co-doping  $\text{Ce}^{3+}$  ions owing to the efficient energy transfer between  $\text{Ce}^{3+}$  and  $\text{Er}^{3+}:$  $^4\text{I}_{11/2}(\text{Er}^{3+}) + ^2\text{F}_{5/2}(\text{Ce}^{3+}) \rightarrow ^4\text{I}_{13/2}(\text{Er}^{3+}) + ^2\text{F}_{7/2}(\text{Ce}^{3+})$  [20]. The other strategy is to decrease the defects on the surface of NPs through growing an inert shell (the shell and the core NPs have similar lattice constants) around the core NPs [21–25]. Bo et al. reported that the intensity of the 1540 nm emission of  $\text{LaF}_3:\text{Yb}^{3+}, \text{Er}^{3+}$  core NPs was enhanced after coating a  $\text{LaF}_3$  inert shell since the coating inert shell method can suppress the surface quenching effect. [26]. The last strategy is to increase the rate of the pump light through coating an active shell (e.g., the shell containing  $\text{Yb}^{3+}$  ions) on the core NPs [27–31]. Zhai et al. reported a method to improve the intensity  $\text{BaYF}_5:\text{Yb}^{3+}, \text{Er}^{3+}$  NPs at 1.53  $\mu\text{m}$  through doping  $\text{Yb}^{3+}$  ions into the  $\text{BaYF}_5$  shell.  $\text{BaYF}_5:\text{Yb}^{3+}, \text{Er}^{3+}@\text{BaYF}_5:\text{Yb}^{3+}$  inert-core-active-shell NPs were obtained and the intensity of the 1.53  $\mu\text{m}$  was enhanced when compared to the  $\text{BaYF}_5:\text{Yb}^{3+}, \text{Er}^{3+}$  core NPs [32]. Despite, recent progress in this field, it is necessary to explore new approaches to achieve small NPs with strong down-conversion luminescence at 1.5  $\mu\text{m}$  for applications regarding near infrared optical communication networks.

In this paper, we choose  $\text{BaLuF}_5$  as the matrix since its phase is a single crystalline phase [33]. We prepared  $\text{BaLuF}_5:\text{Yb}^{3+}, \text{Er}^{3+}, \text{Ce}^{3+}$  NPs by a high-boiling solvent method and studied the effect of the  $\text{Ce}^{3+}$  concentration on the up-conversion (UC) emission and down-conversion (DC) emission (at 1.5  $\mu\text{m}$ ) of  $\text{BaLuF}_5:\text{Yb}^{3+}, \text{Er}^{3+}$  NPs. We synthesized  $\text{BaLuF}_5:\text{Yb}^{3+}, \text{Er}^{3+}, \text{Ce}^{3+}@\text{BaLuF}_5:\text{Yb}^{3+}$  core-shell NPs via growing a  $\text{BaLuF}_5:\text{Yb}^{3+}$  shell and investigated the effect of the  $\text{Yb}^{3+}$  concentration of the shell on the 1.5  $\mu\text{m}$  emission of the  $\text{BaLuF}_5$  core-shell NPs. Finally, we compounded multi-layer  $\text{BaLuF}_5$  core-shell NPs via a layer-by-layer strategy, and obtained  $\text{BaLuF}_5:\text{Yb}^{3+}, \text{Er}^{3+}, \text{Ce}^{3+}@\text{BaLuF}_5:\text{Yb}^{3+}@\text{BaLuF}_5:\text{Yb}^{3+}$  core-active-shell active-shell NPs with a strong down-conversion luminescence at 1.5  $\mu\text{m}$ .

## 2. Materials and Methods

All chemicals were used directly without further purification.  $\text{Lu}(\text{NO}_3)_3 \cdot 6\text{H}_2\text{O}$ ,  $\text{Yb}(\text{NO}_3)_3 \cdot 6\text{H}_2\text{O}$ ,  $\text{Er}(\text{NO}_3)_3 \cdot 6\text{H}_2\text{O}$ , and  $\text{Ce}(\text{NO}_3)_3 \cdot 6\text{H}_2\text{O}$  were purchased from Sigma-Aldrich Chemicals (Shanghai, China). Oleic acid (OA), 1-octadecene (ODE) and Barium stearate were obtained by Alfa Aesar Company (Shanghai, China). NaOH,  $\text{NH}_4\text{F}$  and stearic acid ( $\text{C}_{17}\text{H}_{35}\text{COOH}$ ) were obtained from China National Pharmaceutical Group Corporation (Beijing, China).

### 2.1. Preparation of $\text{BaLuF}_5:\text{Yb}^{3+}, \text{Er}^{3+}$ NPs and $\text{BaLuF}_5:\text{Yb}^{3+}, \text{Er}^{3+}$ Core-Shell NPs

Synthesis of rare-earth stearate: 10 mmol rare-earth nitrate ( $\text{Lu}(\text{NO}_3)_3 \cdot 6\text{H}_2\text{O}$ ,  $\text{Yb}(\text{NO}_3)_3 \cdot 6\text{H}_2\text{O}$ ,  $\text{Er}(\text{NO}_3)_3 \cdot 6\text{H}_2\text{O}$ , or  $\text{Ce}(\text{NO}_3)_3 \cdot 6\text{H}_2\text{O}$ ) and 10 mmol stearic acid were dissolved in 120 mL ethanol, and the system was kept at 80 °C for 30 min. Then, a 20 mL NaOH solution (containing 1.2 g NaOH) was added dropwise into the system. The resulting mixture was refluxed at 80 °C for another 10 h. The reaction product was washed with water and ethanol [34].

Synthesis of  $\text{BaLuF}_5$  nanoparticles: 0.5 mmol barium stearates, 0.5 mmol pre-prepared rare-earth stearate ( $\text{Re}(\text{C}_{17}\text{H}_{35}\text{COO})_3$ ), 15 mL ODE, and 15 mL OA were added to a four-neck round-bottom reaction vessel. After the reaction, the mixture was heated to 150 °C for 30 min under an argon (Ar) flow. A 10 mmol methanol solution containing 0.12g  $\text{NH}_4\text{F}$  was added dropwise into the reaction mixture, and the reaction mixture was heated to 50 °C for 30 min. Then, the reaction mixture was rapidly heated to 300 °C for 1 h and cooled to room temperature (RT) under an Ar flow. The reaction product was washed with cyclohexane and ethanol [31]. The finally obtained nanoparticles were dispersed into cyclohexane.

Synthesis of  $\text{BaLuF}_5$  core-shell nanoparticles: 0.5 mmol barium stearates, 0.5 mmol pre-prepared rare-earth stearate ( $\text{Re}(\text{C}_{17}\text{H}_{35}\text{COO})_3$ ), 15 mL ODE, and 15 mL OA were added to a four-neck round-bottom reaction vessel. The reaction system was heated to 150 °C for 30 min under an Ar flow. After the reaction system was cooled down to 60 °C. The core nanoparticles cyclohexane solution was added into the reaction system with vigorous stirring. A 10 mmol methanol solution containing

0.12 g  $\text{NH}_4\text{F}$  was added dropwise into the reaction system, and the system was heated to  $50\text{ }^\circ\text{C}$  for 30 min. Then the reaction mixture was rapidly heated to  $300\text{ }^\circ\text{C}$  for 1 h and cooled to RT under an Ar flow. The reaction product was washed with cyclohexane and ethanol.

Synthesis of  $\text{BaLuF}_5$  core-shell-shell nanoparticles: To coat the second layer of the shell, these as-synthesized core-shell NPs were used as seeds. The same coating process was repeated.  $\text{BaLuF}_5$  core-shell-shell nanoparticles were obtained.

## 2.2. Characterization

The X-ray powder diffraction (XRD, Rigaku, Japan) were collected by Model Rigaku Ru-200b with  $\text{Cu K}\alpha$  (40 kV, 40 Ma) irradiation ( $\lambda = 1.5406\text{ \AA}$ ). The scan range was set from  $10^\circ$  to  $70^\circ$ . The morphology of the particles was characterized by a JEM-2100F electron microscope (Tokyo, Japan) at 200 kV. The up-conversion spectra of the samples were recorded by a Hitachi F-4500 fluorescence spectrophotometer (Tokyo, Japan) at room temperature under the excitation of a 980 nm laser diode with a fixed power density of  $70\text{ W}\cdot\text{cm}^{-2}$  (1.0 nm for slit resolution and 700 V for PMT voltage). The DC spectra of the samples were collected by a SPEX 1000M spectrometer (HORIBA Group, Kyoto, Japan) at room temperature under the excitation of a 980 nm laser diode with a fixed power density of  $70\text{ W}\cdot\text{cm}^{-2}$  (2 mm for slit width).

## 3. Results and Discussion

### 3.1. Crystal Structure and Morphology

The XRD patterns of the  $\text{BaLuF}_5:18\%\text{Yb}^{3+},2\%\text{Er}^{3+}$  NPs,  $\text{BaLuF}_5:18\%\text{Yb}^{3+},2\%\text{Er}^{3+},2\%\text{Ce}^{3+}$  NPs,  $\text{BaLuF}_5:18\%\text{Yb}^{3+},2\%\text{Er}^{3+},2\%\text{Ce}^{3+}@ \text{BaLuF}_5$  core-inert-shell NPs,  $\text{BaLuF}_5:18\%\text{Yb}^{3+},2\%\text{Er}^{3+},2\%\text{Ce}^{3+}@ \text{BaLuF}_5:5\%\text{Yb}^{3+}$  core-active-shell NPs and  $\text{BaLuF}_5:18\%\text{Yb}^{3+},2\%\text{Er}^{3+},2\%\text{Ce}^{3+}@ \text{BaLuF}_5:5\%\text{Yb}^{3+}@ \text{BaLuF}_5:5\%\text{Yb}^{3+}$  core-active-shell active-shell NPs are shown in Figure 1. It shows that all the diffraction peaks of the samples were well-assigned to the tetragonal phase  $\text{BaGdF}_5$  (JCPDS No. 24-0098), which indicates that the samples are  $\text{BaLuF}_5$  nanoparticles. To characterize the morphology of the samples, we also measured the TEM images of the above samples, and the results are shown in Figure 2. From the TEM image (Figure 2), it is easily seen that the samples are round without agglomeration. The average sizes of  $\text{BaLuF}_5:\text{Yb}^{3+},\text{Er}^{3+}$  core-only NPs and  $\text{BaLuF}_5:\text{Yb}^{3+},\text{Er}^{3+},\text{Ce}^{3+}$  core-only NPs were both about 6 nm, and the above results show that the doping  $\text{Ce}^{3+}$  ions have not changed the size of  $\text{BaLuF}_5$  core-only NPs. The average size of the  $\text{BaLuF}_5$  core-active-shell NPs was about 8 nm after the epitaxial growth of a shell layer. The size of the  $\text{BaLuF}_5$  core-active-shell-active-shell NPs was further increased to about 10 nm after the growth of two shell layers. The particle diameter of nanoparticles was calculated from the XRD pattern, according to the Scherrer equation, and the samples were calculated by the particle size ranges of the nanoparticles at 6 nm, 6 nm, 8 nm, and 10.3 nm. The calculated sizes coincided with the TEM results. The above results indicated that the NPs had a uniform morphology and the average sizes of the shells had not changed.

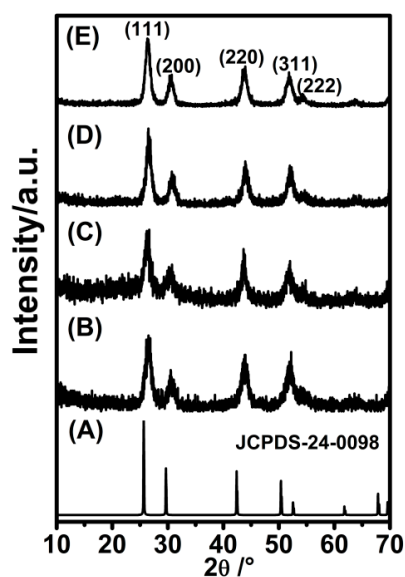


**Figure 1.** X-ray powder diffraction (XRD) patterns of (A) standard BaGdF<sub>5</sub> NPs (the vertical bars denote the standard data for tetragonal structure of bulk BaGdF<sub>5</sub> NPs (JCPDS-24-0098)); (B) BaLuF<sub>5</sub>:18%Yb<sup>3+</sup>,2%Er<sup>3+</sup> core NPs; (C) BaLuF<sub>5</sub>:18%Yb<sup>3+</sup>,2%Er<sup>3+</sup>,2%Ce<sup>3+</sup> core NPs; (D) BaLuF<sub>5</sub>:18%Yb<sup>3+</sup>,2%Er<sup>3+</sup>,2%Ce<sup>3+</sup>@BaLuF<sub>5</sub>:5%Yb<sup>3+</sup> core-active-shell NPs; and (E) BaLuF<sub>5</sub>:18%Yb<sup>3+</sup>,2%Er<sup>3+</sup>,2%Ce<sup>3+</sup>@BaLuF<sub>5</sub>:5%Yb<sup>3+</sup>@BaLuF<sub>5</sub>:5%Yb<sup>3+</sup> core-active-shell-active-shell NPs.

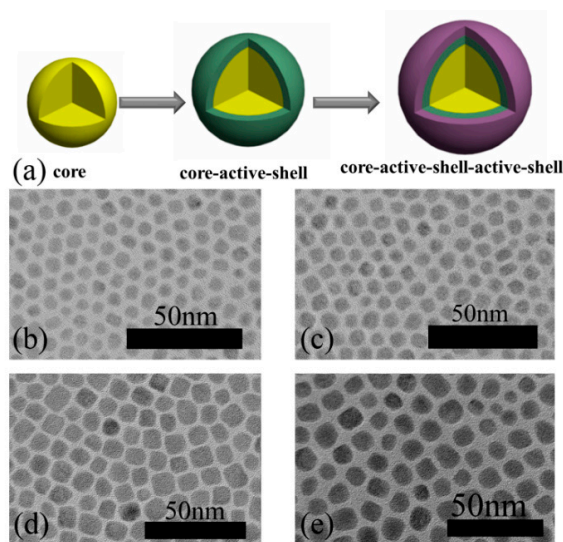


**Figure 2.** (a) Schematic illustration of BaLuF<sub>5</sub> core NPs, BaLuF<sub>5</sub> core-active-shell NPs and BaLuF<sub>5</sub> core-active-shell-active-shell NPs. TEM images of (b) BaLuF<sub>5</sub>:18%Yb<sup>3+</sup>,2%Er<sup>3+</sup> core NPs; (c) BaLuF<sub>5</sub>:18%Yb<sup>3+</sup>,2%Er<sup>3+</sup>,2%Ce<sup>3+</sup> core NPs; (d) BaLuF<sub>5</sub>:18%Yb<sup>3+</sup>,2%Er<sup>3+</sup>,2%Ce<sup>3+</sup>@BaLuF<sub>5</sub>:5%Yb<sup>3+</sup> core-active-shell NPs; and (e) BaLuF<sub>5</sub>:18%Yb<sup>3+</sup>,2%Er<sup>3+</sup>,2%Ce<sup>3+</sup>@BaLuF<sub>5</sub>:5%Yb<sup>3+</sup>@BaLuF<sub>5</sub>:5%Yb<sup>3+</sup> core-active-shell-active-shell NPs.

### 3.2. Optical Properties

#### 3.2.1. Effect of Ce<sup>3+</sup> Concentration on the Luminescence Properties of BaLuF<sub>5</sub>:Yb<sup>3+</sup>,Er<sup>3+</sup> NPs

In BaLuF<sub>5</sub>:Yb<sup>3+</sup>,Er<sup>3+</sup>,Ce<sup>3+</sup> systems, all the energy transfer processes are shown in the Figure 3. With the excitation of a 980 nm laser diode, the Yb<sup>3+</sup> ions are excited from the <sup>2</sup>F<sub>7/2</sub> level to the <sup>2</sup>F<sub>5/2</sub> level and then transfer the energy to Er<sup>3+</sup> to populate higher energy levels of the Er<sup>3+</sup> ions:<sup>4</sup>H<sub>11/2</sub>

level,  ${}^4F_{9/2}$ , and  ${}^4F_{7/2}$ . The  ${}^4H_{11/2} \rightarrow {}^4I_{15/2}$  ( $\approx 525$  nm),  ${}^4S_{3/2} \rightarrow {}^4I_{15/2}$  ( $\approx 545$  nm), and  ${}^4F_{9/2} \rightarrow {}^4I_{15/2}$  ( $\approx 655$  nm) transitions gives the UC emission, and the  ${}^4I_{13/2} \rightarrow {}^4I_{15/2}$  transition gives the DC emission at 1.53  $\mu\text{m}$ . Interestingly, with the addition of  $\text{Ce}^{3+}$  ions, the energy transfer occurs between  $\text{Ce}^{3+}$  and  $\text{Er}^{3+}$ :  ${}^4I_{11/2} (\text{Er}^{3+}) + {}^2F_{5/2} (\text{Ce}^{3+}) \rightarrow {}^4I_{13/2} (\text{Er}^{3+}) + {}^2F_{7/2} (\text{Ce}^{3+})$ . Furthermore, the  ${}^4I_{11/2}$  state of  $\text{Er}^{3+}$  ions populate the  ${}^4I_{13/2}$  state [17,35–37]. The intensity of the DC emission is enhanced and that of the UC emission are suppressed by the addition of  $\text{Ce}^{3+}$  ions.

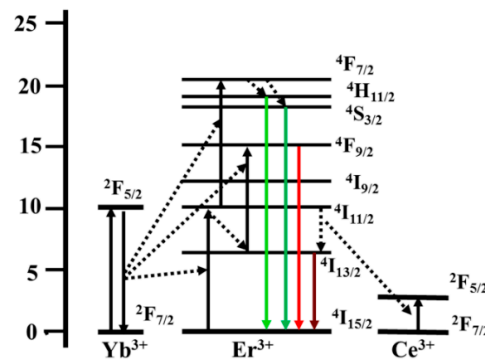


**Figure 3.** Diagram of energy levels of  $\text{Yb}^{3+}\text{-Er}^{3+}\text{-Ce}^{3+}$  and up-conversion (UC) emission and down-conversion (DC) emission processes in the  $\text{BaLuF}_5:\text{Yb}^{3+}, \text{Er}^{3+}, \text{Ce}^{3+}$  systems under 980 nm excitation.

In order to investigate the effect of  $\text{Ce}^{3+}$  ion on the UC emission, we measured the UC emission spectra of  $\text{BaLuF}_5:18\%\text{Yb}^{3+}, 2\%\text{Er}^{3+}, x\%\text{Ce}^{3+}$  NPs with different  $\text{Ce}^{3+}$  concentrations ( $x = 0, 1, 2, 3,$  and  $4$ ) under the excitation of a 980 nm laser diode, and the data is shown in Figure 4a. All samples exhibit several UC emission peaks, which are attributed to the  ${}^4H_{11/2} \rightarrow {}^4I_{15/2}$  ( $\approx 525$  nm),  ${}^4S_{3/2} \rightarrow {}^4I_{15/2}$  ( $\approx 545$  nm), and  ${}^4F_{9/2} \rightarrow {}^4I_{15/2}$  ( $\approx 655$  nm) transitions of  $\text{Er}^{3+}$  ions, respectively. When the  $\text{Ce}^{3+}$  concentration was 0%, the UC luminescence of  $\text{BaLuF}_5:\text{Yb}^{3+}, \text{Er}^{3+}$  NPs was the strongest one. It is clear that the intensity of the UC emissions decreased gradually with the increase of  $\text{Ce}^{3+}$  concentration from 0% to 2% (as shown in Figure 4b). This is due to the following energy transfer occurring between  $\text{Ce}^{3+}$  and  $\text{Er}^{3+}$ :  ${}^4I_{11/2} (\text{Er}^{3+}) + {}^2F_{5/2} (\text{Ce}^{3+}) \rightarrow {}^4I_{13/2} (\text{Er}^{3+}) + {}^2F_{7/2} (\text{Ce}^{3+})$  [17,35–37]. However, when the concentration of  $\text{Ce}^{3+}$  ions reached 4%, the intensity of the UC emissions increased monotonically (as shown in Figure 4b). The above results show that doping  $\text{Ce}^{3+}$  ions led to the suppression of the UC emissions of  $\text{Er}^{3+}$  ions.

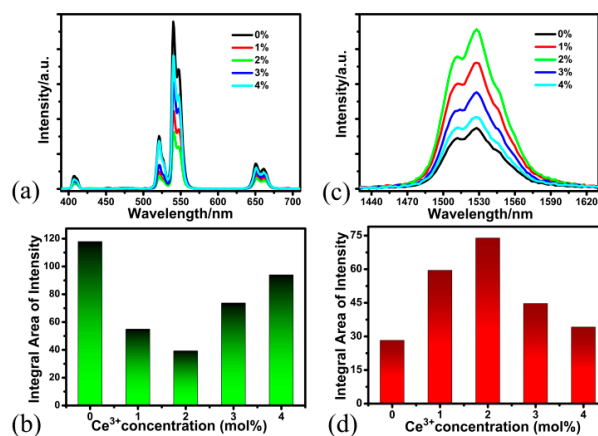


**Figure 4.** (a) UC and (c) DC emission spectra of  $\text{BaLuF}_5:18\%\text{Yb}^{3+}, 2\%\text{Er}^{3+}, x\%\text{Ce}^{3+}$  NPs with different  $\text{Ce}^{3+}$  concentrations ( $x = 0, 1, 2, 3,$  and  $4$ ) under the excitation of a 980 nm laser diode. Intensity enhancement of (b) UC and (d) DC emission depending on the  $\text{Ce}^{3+}$  concentrations in  $\text{BaLuF}_5:18\%\text{Yb}^{3+}, 2\%\text{Er}^{3+}, x\%\text{Ce}^{3+}$  NPs.

In addition, we also studied the influence of the  $\text{Ce}^{3+}$  concentration on the DC luminescence of  $\text{BaLuF}_5:\text{Yb}^{3+},\text{Er}^{3+}$  NPs.  $\text{BaLuF}_5:18\%\text{Yb}^{3+},2\%\text{Er}^{3+},x\%\text{Ce}^{3+}$  ( $x = 0, 1, 2, 3,$  and  $4$ ) NPs were synthesized using a high-boiling solvent method. Figure 4c shows the DC emission of the  $^4\text{I}_{13/2} \rightarrow ^4\text{I}_{15/2}$  transition of  $\text{Er}^{3+}$  ions with varying  $\text{Ce}^{3+}$  concentration under the excitation of a 980 nm laser. We found that the intensity of the DC luminescence gradually increased with increasing  $\text{Ce}^{3+}$  concentration from 0% to 2% (as shown in Figure 4d). This may be due to the branching ratio of the  $\text{Er}^{3+}:^4\text{I}_{11/2} \rightarrow ^4\text{I}_{13/2}$  transition, which can be increased by doping with  $\text{Ce}^{3+}$  ions, and the energy transfer process can increase the population of  $^4\text{I}_{13/2}$  state of  $\text{Er}^{3+}$  ions through the following energy transfer process:  $^4\text{I}_{11/2} (\text{Er}^{3+}) + ^2\text{F}_{5/2} (\text{Ce}^{3+}) \rightarrow ^4\text{I}_{13/2} (\text{Er}^{3+}) + ^2\text{F}_{7/2} (\text{Ce}^{3+})$  [17,35–37]. The results led to the enhancement of the DC emission of  $\text{Er}^{3+}$  ions. Meanwhile, the intensity of the DC emissions reduced monotonically with increasing  $\text{Ce}^{3+}$  concentration from 2% to 4% (as shown in Figure 4d), since the cross relaxation:  $\text{Er}^{3+}:^4\text{I}_{13/2} + \text{Ce}^{3+}: ^2\text{F}_{5/2} \rightarrow \text{Er}^{3+}:^4\text{I}_{15/2} + \text{Ce}^{3+}: ^2\text{F}_{7/2}$  happened. These results indicate that when the concentration of  $\text{Ce}^{3+}$  ions was 2%, the intensity of the DC luminescence reached its maximum. The DC emissions of  $\text{BaLuF}_5:18\%\text{Yb}^{3+},2\%\text{Er}^{3+},2\%\text{Ce}^{3+}$  NPs were about 2.6 times compared to that of  $\text{BaLuF}_5:18\%\text{Yb}^{3+},2\%\text{Er}^{3+}$  NPs, which means that doping  $\text{Ce}^{3+}$  ions led to the enhancement of the DC emissions of  $\text{Er}^{3+}$  ions. Thus, the optimum concentration of  $\text{Er}^{3+}$  was about 2% for tri-doped  $\text{BaLuF}_5$  NPs.

### 3.2.2. Effect of $\text{Yb}^{3+}$ Concentration of the Shell on the DC Luminescence Properties of $\text{BaLuF}_5:\text{Yb}^{3+},\text{Er}^{3+},\text{Ce}^{3+}@\text{BaLuF}_5:\text{Yb}^{3+}$ Core-Shell NPs

Here, we choose  $\text{BaLuF}_5:18\%\text{Yb}^{3+},2\%\text{Er}^{3+},2\%\text{Ce}^{3+}$  NPs as the core, and prepared  $\text{BaLuF}_5:18\%\text{Yb}^{3+},2\%\text{Er}^{3+},2\%\text{Ce}^{3+}@\text{BaLuF}_5:x\%\text{Yb}^{3+}$  ( $x = 0, 2.5, 5, 7.5$  and  $10$ ) core-shell NPs. To clarify the effects of  $\text{Yb}^{3+}$  concentration on the shell on the DC luminescence properties of  $\text{BaLuF}_5:18\%\text{Yb}^{3+},2\%\text{Er}^{3+},2\%\text{Ce}^{3+}@\text{BaLuF}_5:\text{Yb}^{3+}$  core-shell NPs, we measured the DC emission spectra of the core-shell NPs with different  $\text{Yb}^{3+}$  concentrations (0%, 2.5%, 5%, 7.5%, and 10%) under a 980 nm laser excitation, and the measured data is shown in Figure 5a. We can see from the Figure 5a that  $\text{BaLuF}_5:\text{Yb}^{3+},\text{Er}^{3+}$  core NPs and  $\text{BaLuF}_5:\text{Yb}^{3+},\text{Er}^{3+},\text{Ce}^{3+}$  core NPs show the weakest emission peak at 1530 nm. The main reason is that the surface area-to-volume ratio of the core-only NPs was very high and a large portion of the dopants should be located at the surface. Hence, the energy from the pump light will be easily quenched by the surface defects of the core-only NPs. The luminescence intensity of  $\text{BaLuF}_5$  core-inert-shell NPs was obviously increased after the  $\text{BaLuF}_5$  insert shell. The luminescence intensity of  $\text{BaLuF}_5$  core-inert-shell NPs was increased by 3.7 times compared to that of the  $\text{BaLuF}_5:\text{Yb}^{3+},\text{Er}^{3+}$  core NPs with doping  $\text{Ce}^{3+}$  ions. This is because the insert shell can suppress the nonradiative transitions [23,24]. Interestingly, when the shell was doped with  $\text{Yb}^{3+}$  ions, the luminescence intensity of the  $\text{BaLuF}_5:\text{Yb}^{3+},\text{Er}^{3+},\text{Ce}^{3+}$  core-active-shell NPs could be increased further compared to that of the  $\text{BaLuF}_5:\text{Yb}^{3+},\text{Er}^{3+},\text{Ce}^{3+}$  core-inert-shell NPs. The luminescence intensity of the  $\text{BaLuF}_5:\text{Yb}^{3+},\text{Er}^{3+},\text{Ce}^{3+}$  core-active-shell NPs monotonically enhanced with increasing of  $\text{Yb}^{3+}$  concentration in the shell from 0% to 5% (as shown in Figure 5b). However, when the  $\text{Yb}^{3+}$  concentration in the shell was 5%, the luminescence intensity of the  $\text{BaLuF}_5$  core-shell NPs reached its maximum value. This was due to the  $\text{Yb}^{3+}$  ions in the shell could transfer energy from the pump source to the core and make a contribution to the DC emissions [31]. When the  $\text{Yb}^{3+}$  concentration in the shell continuously increased from 5% to 10%, the luminescence intensity of the  $\text{BaLuF}_5:\text{Yb}^{3+},\text{Er}^{3+},\text{Ce}^{3+}$  core-active-shell NPs gradually decreased since the concentration quenching effect occurred [31,38]. These results indicate that the optimum concentration of  $\text{Yb}^{3+}$  in the shell was about 5% for  $\text{BaLuF}_5:\text{Yb}^{3+},\text{Er}^{3+},\text{Ce}^{3+}$  core-active-shell NPs, the intensity of the UC emissions of  $\text{BaLuF}_5:\text{Yb}^{3+},\text{Er}^{3+},\text{Ce}^{3+}@\text{BaLuF}_5:\text{Yb}^{3+}$  core-active-shell NPs was increased by 9.4 times compared that of the  $\text{BaLuF}_5:\text{Yb}^{3+},\text{Er}^{3+},\text{Ce}^{3+}$  core NPs, and was increased by 24.6 times compared to that of the  $\text{BaLuF}_5:\text{Yb}^{3+},\text{Er}^{3+}$  core NPs without doping  $\text{Ce}^{3+}$  ions.

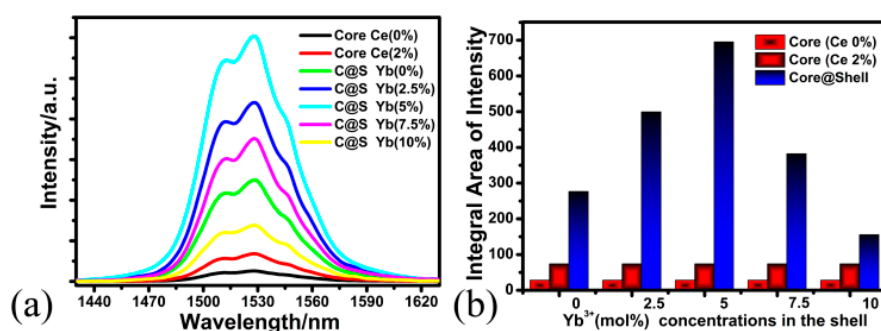


**Figure 5.** (a) DC emission spectra of BaLuF<sub>5</sub>:18%Yb<sup>3+</sup>,2%Er<sup>3+</sup> core NPs, BaLuF<sub>5</sub>:18%Yb<sup>3+</sup>,2%Er<sup>3+</sup>,2%Ce<sup>3+</sup> core NPs and BaLuF<sub>5</sub>:18%Yb<sup>3+</sup>,2%Er<sup>3+</sup>,2%Ce<sup>3+</sup>@BaLuF<sub>5</sub>:x%Yb<sup>3+</sup> NPs (x = 0, 2.5, 5, 7.5 and 10) core-active-shell NPs under the excitation of a 980 nm laser diode. (b) Intensity enhancement of DC emission depending on the Yb<sup>3+</sup> concentrations in BaLuF<sub>5</sub> core-active-shell NPs.

### 3.2.3. Synthesis of BaLuF<sub>5</sub>:Yb<sup>3+</sup>,Er<sup>3+</sup>,Ce<sup>3+</sup>@BaLuF<sub>5</sub>:Yb<sup>3+</sup>@BaLuF<sub>5</sub>:Yb<sup>3+</sup> Core-Shell-Shell NPs with Strong Down-Conversion Luminescence

In order to get the tri-doped BaLuF<sub>5</sub>:Yb<sup>3+</sup>,Er<sup>3+</sup>,Ce<sup>3+</sup> core-shell NPs with strong DC luminescence, we synthesized BaLuF<sub>5</sub>:18%Yb<sup>3+</sup>,2%Er<sup>3+</sup>,2%Ce<sup>3+</sup>@BaLuF<sub>5</sub>:5%Yb<sup>3+</sup>@BaLuF<sub>5</sub>:5%Yb<sup>3+</sup> core-shell-shell NPs via a high boiling solvent process through a layer-by-layer strategy. Figure 6c shows the DC emission of BaLuF<sub>5</sub>:18%Yb<sup>3+</sup>,2%Er<sup>3+</sup> core NPs, BaLuF<sub>5</sub>:18%Yb<sup>3+</sup>,2%Er<sup>3+</sup>,2%Ce<sup>3+</sup> core NPs, BaLuF<sub>5</sub>:18%Yb<sup>3+</sup>,2%Er<sup>3+</sup>,2%Ce<sup>3+</sup>@BaLuF<sub>5</sub>:5%Yb<sup>3+</sup> core-active-shell NPs and BaLuF<sub>5</sub>:18%Yb<sup>3+</sup>,2%Er<sup>3+</sup>,2%Ce<sup>3+</sup>@BaLuF<sub>5</sub>:5%Yb<sup>3+</sup>@BaLuF<sub>5</sub>:5%Yb<sup>3+</sup> core-active-shell-active-shell NPs under the excitation of a 980 nm laser diode. The DC emission intensity of BaLuF<sub>5</sub> core NPs without doping Ce<sup>3+</sup> ions shows the weakest DC emission. By doping with Ce<sup>3+</sup> ions, the luminescence intensity of the BaLuF<sub>5</sub>:Yb<sup>3+</sup>,Er<sup>3+</sup>,Ce<sup>3+</sup> core NPs was 2.6 times more than that of BaLuF<sub>5</sub>:Yb<sup>3+</sup>,Er<sup>3+</sup> core NPs due to the energy transfer between Er<sup>3+</sup> and Ce<sup>3+</sup>. After, by growing an BaLuF<sub>5</sub>:5%Yb<sup>3+</sup> active shell, the DC emission intensity of the BaLuF<sub>5</sub>:Yb<sup>3+</sup>,Er<sup>3+</sup>,Ce<sup>3+</sup> core-active-shell NPs was further enhanced, since the active shell could be used to not only suppress surface quenching but also transfer energy from the pump light to the core region efficiently through Yb<sup>3+</sup> ions inside the active shells. When the number of the active shell layers reaches two, the DC emission intensity of the BaLuF<sub>5</sub>:Yb<sup>3+</sup>,Er<sup>3+</sup>,Ce<sup>3+</sup> core-active-shell-active-shell NPs was 16.8 times more than that of BaLuF<sub>5</sub>:Yb<sup>3+</sup>,Er<sup>3+</sup>,Ce<sup>3+</sup> core NPs. This was because the size of the active shell was too small to completely suppress surface quenching, and coating two active shell layers could effectively suppress surface quenching [31]. In the last, we got BaLuF<sub>5</sub>:18%Yb<sup>3+</sup>,2%Er<sup>3+</sup>,2%Ce<sup>3+</sup>@BaLuF<sub>5</sub>:5%Yb<sup>3+</sup>@BaLuF<sub>5</sub>:5%Yb<sup>3+</sup> core-active-shell-active-shell NPs with the strong DC luminescence at 1.5 μm. The DC emission intensity of the BaLuF<sub>5</sub>:18%Yb<sup>3+</sup>,2%Er<sup>3+</sup>,2%Ce<sup>3+</sup>@BaLuF<sub>5</sub>:5%Yb<sup>3+</sup>@BaLuF<sub>5</sub>:5%Yb<sup>3+</sup> core-active-shell-active-shell NPs was 44 times more than that of BaLuF<sub>5</sub>:Yb<sup>3+</sup>,Er<sup>3+</sup> core NPs without the dopant Ce<sup>3+</sup> ions. Besides, we measured the photo stability of the BaLuF<sub>5</sub>:18%Yb<sup>3+</sup>,2%Er<sup>3+</sup>,2%Ce<sup>3+</sup>@BaLuF<sub>5</sub>:5%Yb<sup>3+</sup>@BaLuF<sub>5</sub>:5%Yb<sup>3+</sup> core-active-shell-active-shell NPs (as shown in Figure S1). Those results show that the core-active-shell-active-shell NPs have optical stability.

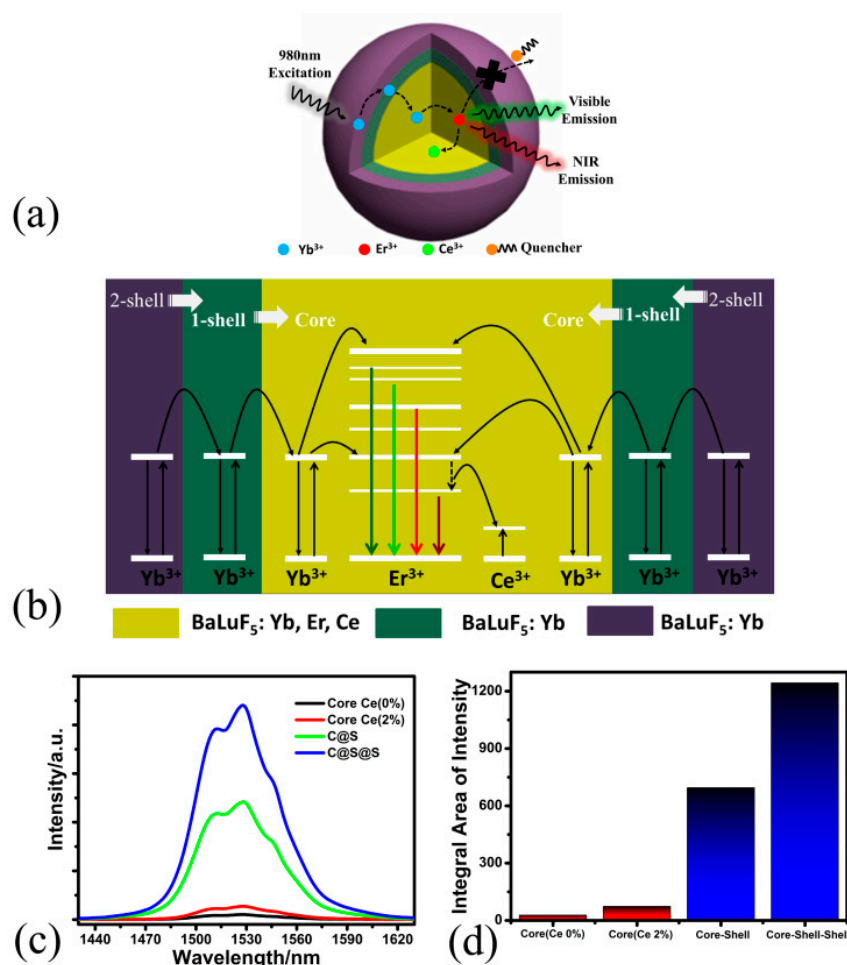


**Figure 6.** (a) Schematic illustration and (b) energy transfer mechanisms of  $\text{BaLuF}_5:18\%\text{Yb}^{3+}, 2\%\text{Er}^{3+}, 2\%\text{Ce}^{3+}@ \text{BaLuF}_5:5\%\text{Yb}^{3+}@ \text{BaLuF}_5:5\%\text{Yb}^{3+}$  core-active-shell-active-shell NPs. (c) DC emission spectra of  $\text{BaLuF}_5:18\%\text{Yb}^{3+}, 2\%\text{Er}^{3+}$  core NPs,  $\text{BaLuF}_5:18\%\text{Yb}^{3+}, 2\%\text{Er}^{3+}, 2\%\text{Ce}^{3+}$  core NPs,  $\text{BaLuF}_5:18\%\text{Yb}^{3+}, 2\%\text{Er}^{3+}, 2\%\text{Ce}^{3+}@ \text{BaLuF}_5:5\%\text{Yb}^{3+}$  core-active-shell NPs and  $\text{BaLuF}_5:18\%\text{Yb}^{3+}, 2\%\text{Er}^{3+}, 2\%\text{Ce}^{3+}@ \text{BaLuF}_5:5\%\text{Yb}^{3+}@ \text{BaLuF}_5:5\%\text{Yb}^{3+}$  core-active-shell-active-shell NPs. (d) Intensity enhancement of DC emission in all the above NPs.

In addition, we measured the lifetime of the  $^4\text{I}_{13/2}$  level of  $\text{Er}^{3+}$  in  $\text{BaLuF}_5:18\%\text{Yb}^{3+}, 2\%\text{Er}^{3+}$  NPs,  $\text{BaLuF}_5:18\%\text{Yb}^{3+}, 2\%\text{Er}^{3+}, 2\%\text{Ce}^{3+}$  NPs,  $\text{BaLuF}_5:18\%\text{Yb}^{3+}, 2\%\text{Er}^{3+}, 2\%\text{Ce}^{3+}@ \text{BaLuF}_5:5\%\text{Yb}^{3+}$  NPs, and  $\text{BaLuF}_5:18\%\text{Yb}^{3+}, 2\%\text{Er}^{3+}, 2\%\text{Ce}^{3+}@ \text{BaLuF}_5:5\%\text{Yb}^{3+}@ \text{BaLuF}_5:5\%\text{Yb}^{3+}$  NPs by using a 980 nm pulsed laser with a pulse width of 100  $\mu\text{s}$  and a repetition rate of 20 Hz as the excitation source. The result is shown in Figure 7. Each of the decay curves could be fitted well with a single-exponential function as  $I = I_0 \exp(-t/\tau)$ , where  $I_0$  is the initial emission intensity at  $t = 0$  and  $\tau$  is the lifetime of the monitored level. Obviously, the lifetime of the  $^4\text{I}_{13/2}$  level of  $\text{Er}^{3+}$  was extended from 517  $\mu\text{s}$  to 579  $\mu\text{s}$  by introducing  $\text{Ce}^{3+}$  ions into the  $\text{BaLuF}_5: \text{Yb}^{3+}, \text{Er}^{3+}$  core NPs. This was because the quenching of  $\text{Er}^{3+}$  ions from the  $^4\text{I}_{11/2}$  state to the  $^4\text{I}_{13/2}$  state by the energy transfer occurs between  $\text{Ce}^{3+}$  and  $\text{Er}^{3+}$ :  $^4\text{I}_{11/2} (\text{Er}^{3+}) + ^2\text{F}_{5/2} (\text{Ce}^{3+}) \rightarrow ^4\text{I}_{13/2} (\text{Er}^{3+}) + ^2\text{F}_{7/2} (\text{Ce}^{3+})$ . Interestingly, by growing a  $\text{BaLuF}_5: 5\% \text{Yb}^{3+}$  shell on the core NP, the lifetime of the  $^4\text{I}_{13/2}$  level was extended from 579  $\mu\text{s}$  to 818  $\mu\text{s}$  owing to the reduction of the nonradiative relaxation rate caused by the surface passivation. When the number of the shell layer reached two, the lifetime of the  $^4\text{I}_{13/2}$  level further increased to 936  $\mu\text{s}$  since the thickness of each shell layer was about 2 nm, and therefore one shell layer was not enough for suppressing surface quenching completely. The result agreed well with the tendency toward the dependence of the measured DC emissions (shown in Figure 6c).

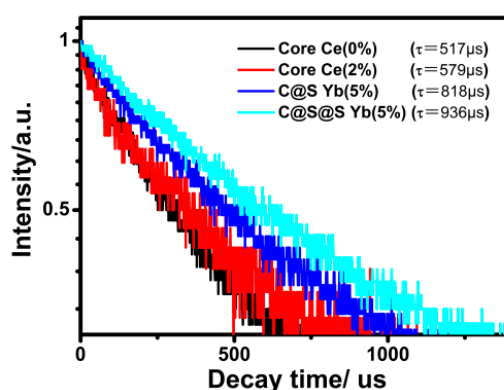


**Figure 7.** The lifetime of the  ${}^4I_{13/2}$  level of  $Er^{3+}$  (monitored at 1530 nm corresponding to the  ${}^4I_{13/2} \rightarrow {}^4I_{13/2}$ ) in  $BaLuF_5:18\%Yb^{3+}, 2\%Er^{3+}$  NPs,  $BaLuF_5:18\%Yb^{3+}, 2\%Er^{3+}, 2\%Ce^{3+}$  NPs,  $BaLuF_5:18\%Yb^{3+}, 2\%Er^{3+}, 2\%Ce^{3+}@BaLuF_5:5\%Yb^{3+}$  NPs, and  $BaLuF_5:18\%Yb^{3+}, 2\%Er^{3+}, 2\%Ce^{3+}@BaLuF_5:5\%Yb^{3+}@BaLuF_5:5\%Yb^{3+}$  NPs by using a 980 nm pulsed laser with a pulse width of 100  $\mu s$  and a repetition rate of 20 Hz as the excitation source.

#### 4. Conclusions

In summary, we synthesized  $BaLuF_5:18\%Yb^{3+}, 2\%Er^{3+}, 2\%Ce^{3+}$  core NPs by introducing  $Ce^{3+}$  ions via a high boiling solvent process. In the case of  $BaLuF_5:18\%Yb^{3+}, 2\%Er^{3+}$  core NPs, the UC emission intensity of  $BaLuF_5:18\%Yb^{3+}, 2\%Er^{3+}, 2\%Ce^{3+}$  core NPs significantly decreased and the DC emission intensity obviously increased due to the energy transfer between  $Er^{3+}$  and  $Ce^{3+}$  ions according to:  ${}^4I_{11/2} (Er^{3+}) + {}^2F_{5/2} (Ce^{3+}) \rightarrow {}^4I_{13/2} (Er^{3+}) + {}^2F_{7/2} (Ce^{3+})$ . We prepared  $BaLuF_5:Yb^{3+}, Er^{3+}, Ce^{3+}$  core-active-shell-active-shell NPs via a layer-by-layer strategy. In comparison with the optical properties of  $BaLuF_5:Yb^{3+}, Er^{3+}$  core NPs, the DC emission intensity of  $BaLuF_5:Yb^{3+}, Er^{3+}, Ce^{3+}$  core-active-shell-active-shell NPs were enhanced by 44 times after coating with two-layer  $BaLuF_5:Yb^{3+}$  active shells. We effectively enhanced the DC emission intensity of  $Yb^{3+}-Er^{3+}$  co-doping  $BaLuF_5$  NPs through introducing  $Ce^{3+}$  ions into  $BaLuF_5$  NPs and multiple  $BaLuF_5:5\%Yb^{3+}$  active-shell coatings.

**Supplementary Materials:** The following are available online at <http://www.mdpi.com/2079-4991/8/8/615/s1>, Figure S1: (a) The intensity change of  $BaLuF_5:18\%Yb^{3+}, 2\%Er^{3+}, 2\%Ce^{3+}@BaLuF_5:5\%Yb^{3+}@BaLuF_5:5\%Yb^{3+}$  NPs core-active-shell-active-shell NPs for 980 nm constant light exposure. (b) The inset shows the DC emission of the core-active-shell-active-shell NPs after 980 nm laser light irradiation for 0 h, 6 h, 12 h, respectively.

**Author Contributions:** Y.Z. conceived and designed the experiments; Y.Z. and Y.S. performed the experiments; Z.Q., M.S., and W.Q. analyzed the data, contributed reagents/materials/analysis tools. Y.Z. wrote the paper. All authors have read and approved the final manuscript.

**Funding:** This research was funded by the Science and technology development plan project of Jilin Province of China (No1. 20180520199JH, No. 2.20180520191JH); Science and technology project of the Jilin Provincial Education Department of China (No. JJKH20180762KJ); The National Natural Science Foundation of China (No. 21701047) and The State Key Laboratory of Rare Earth Resource Utilization, Changchun Institute of Applied Chemistry, Chinese Academy of Sciences (Grant No. RERU2017013).

**Conflicts of Interest:** The authors declare no conflict of interest.

#### References

1. Shan, G.B.; Demopoulos, G.P. Near-infrared sunlight harvesting in dye-sensitized solar cells via the insertion of an upconverter-TiO<sub>2</sub> nanocomposite layer. *J. Adv. Mater.* **2010**, *22*, 4373–4377. [[CrossRef](#)] [[PubMed](#)]
2. Xu, J.; Yang, P.; Sun, M.; Bi, H.; Liu, B.; Yang, D.; Gai, S.; He, F.; Lin, J. Highly emissive dye-sensitized upconversion nanostructure for dual-photosensitizer photodynamic therapy and bioimaging. *J. ACS Nano* **2017**, *11*, 4133–4144. [[CrossRef](#)] [[PubMed](#)]

3. Wang, C.; Xu, C.; Xu, L.; Sun, C.; Yang, D.; Xu, J.; He, F.; Gai, S.; Yang, P. A novel core-shell structured upconversion nanorod as a multimodal bioimaging and photothermal ablation agent for cancer theranostics. *J. Mater. Chem. B* **2018**, *6*, 2597–2607. [[CrossRef](#)]
4. Shen, J.W.; Yang, C.X.; Dong, L.X.; Sun, H.R.; Gao, K.; Yan, X.P. Incorporation of computed tomography and magnetic resonance imaging function into NaYF<sub>4</sub>:Yb/Tm upconversion nanoparticles for in vivo trimodal bioimaging. *J. Anal. Chem.* **2013**, *85*, 12166–12172. [[CrossRef](#)] [[PubMed](#)]
5. Peng, J.; Sun, Y.; Zhao, L.; Wu, Y.; Feng, W.; Gao, Y.; Li, F. Polyphosphoric acid capping radioactive/upconverting NaLuF<sub>4</sub>:Yb,Tm,<sup>153</sup>Sm nanoparticles for blood pool imaging in vivo. *J. Biomater.* **2013**, *34*, 9535–9544. [[CrossRef](#)] [[PubMed](#)]
6. Qin, W.; Zhang, D.; Zhao, D.; Wang, L.; Zheng, K. Near-infrared photocatalysis based on YF<sub>3</sub>:Yb<sup>3+</sup>,Tm<sup>3+</sup>/TiO<sub>2</sub> core/shell nanoparticles. *J. Chem. Commun.* **2010**, *46*, 2304–2306. [[CrossRef](#)] [[PubMed](#)]
7. Wang, F.; Han, Y.; Lim, C.S.; Lu, Y.; Wang, J.; Xu, J.; Chen, H.; Zhang, C.; Hong, M.; Liu, X. Simultaneous phase and size control of upconversion nanocrystals through lanthanide doping. *J. Nature* **2010**, *463*, 1061–1065. [[CrossRef](#)] [[PubMed](#)]
8. De Wild, J.; Rath, J.K.; Meijerink, A.; van Sark, W.G.J.H.M.; Schropp, R.E.I. Enhanced near-infrared response of a-Si:H solar cells with β-NaYF<sub>4</sub>:Yb<sup>3+</sup> (18%),Er<sup>3+</sup> (2%) upconversion phosphors. *J. Sol. Energy Mater. Sol. Cells* **2010**, *94*, 2395–2398. [[CrossRef](#)]
9. Wang, C.; Cheng, L.; Liu, Z. Drug delivery with upconversion nanoparticles for multi-functional targeted cancer cell imaging and therapy. *J. Biomater.* **2011**, *32*, 1110–1120. [[CrossRef](#)] [[PubMed](#)]
10. Bagheri, A.; Arandiyani, H.; Boyer, C.; Lim, M. Lanthanide-doped upconversion nanoparticles: emerging intelligent light-activated drug delivery systems. *J. Adv. Sci.* **2016**, *3*, 1500437. [[CrossRef](#)] [[PubMed](#)]
11. Adusumalli, V.N.K.B.; Sarkar, S.; Mahalingam, V. Strong single-band blue emission from colloidal Ce<sup>3+</sup>/Tm<sup>3+</sup>-doped NaYF<sub>4</sub> nanocrystals for light-emitting applications. *J. ChemPhysChem* **2015**, *16*, 2312–2316. [[CrossRef](#)] [[PubMed](#)]
12. Wu, Y.M.; Cen, Y.; Huang, L.J.; Yu, R.Q.; Chu, X. Upconversion fluorescence resonance energy transfer biosensor for sensitive detection of human immunodeficiency virus antibodies in human serum. *J. Chem. Commun.* **2014**, *50*, 4759–4762. [[CrossRef](#)] [[PubMed](#)]
13. Zhang, M.; Zhang, W.; Fei, W.; Zhao, D.; Qu, C.; Wang, X.; Yi, Y.; Cassan, E.; Zhang, D. High-gain polymer optical waveguide amplifiers based on core-shell NaYF<sub>4</sub>/NaLuF<sub>4</sub>:Yb<sup>3+</sup>,Er<sup>3+</sup> NPs-PMMA covalent-linking nanocomposites. *Sci. Rep.* **2016**, *6*, 36729. [[CrossRef](#)] [[PubMed](#)]
14. Zhang, D.; Chen, C.; Chen, C.; Ma, C.; Zhang, D. Optical gain at 1535 nm in LaF<sub>3</sub>:Er,Yb nanoparticle-doped organic-inorganic hybrid material waveguide. *J. Appl. Phys. Lett.* **2007**, *91*, 161109. [[CrossRef](#)]
15. Lei, K.-L.; Chow, C.-F.; Tsang, K.-C.; Lei, E.N.Y.; Roy, V.A.L.; Lam, M.H.W.; Lee, C.S.; Pun, E.Y.B.; Li, J. Long aliphatic chain coated rare-earth nanocrystal as polymer-based optical waveguide amplifiers. *J. Mater. Chem.* **2010**, *20*, 7526–7529. [[CrossRef](#)]
16. Bo, S.; Wang, J.; Zhao, H.; Ren, H.; Wang, Q.; Xu, G.; Zhang, X.; Liu, X.; Zhen, Z. LaF<sub>3</sub>:Er,Yb doped sol-gel polymeric optical waveguide amplifiers. *J. Appl. Phys. B* **2008**, *91*, 79–83. [[CrossRef](#)]
17. Liu, X.; Qiu, J.; Xu, X.; Zhou, D. Effect of Ce<sup>3+</sup> concentration on the luminescence properties of Ce<sup>3+</sup>/Er<sup>3+</sup>/Yb<sup>3+</sup> tri-doped NaYF<sub>4</sub> nanocrystals. *J. Nanosci. Nanotechnol.* **2016**, *16*, 3749–3753. [[CrossRef](#)] [[PubMed](#)]
18. Khaydukov, K.V.; Rocheva, V.V.; Savelyev, A.G.; Sarycheva, M.E.; Asharchuk, I.M. Synthesis of NaLuF<sub>4</sub>:Er<sup>3+</sup>,Yb<sup>3+</sup>,Ce<sup>3+</sup> nanoparticles and study of photoluminescent properties in C-band. *EPJ Web Conf.* **2017**, *132*, 03049. [[CrossRef](#)]
19. Huang, B.; Zhou, Y.; Yang, F.; Wu, L.; Qi, Y.; Li, J. The 1.53 μm spectroscopic properties of Er<sup>3+</sup>/Ce<sup>3+</sup>/Yb<sup>3+</sup> tri-doped tellurite glasses containing silver nanoparticles. *J. Opt. Mater.* **2016**, *51*, 9–17. [[CrossRef](#)]
20. Zhai, X.; Li, J.; Liu, S.; Liu, X.; Zhao, D.; Wang, F.; Zhang, D.; Qin, G.; Qin, W. Enhancement of 1.53 μm emission band in NaYF<sub>4</sub>:Er<sup>3+</sup>,Yb<sup>3+</sup>,Ce<sup>3+</sup> nanocrystals for polymer-based optical waveguide amplifiers. *J. Opt. Mater. Express* **2013**, *3*, 270–277. [[CrossRef](#)]
21. Chen, G.; Ohulchanskyy, T.Y.; Liu, S.; Law, W.C.; Wu, F.; Swihart, M.T.; Agren, H.; Prasad, P.N. Core/shell NaGdF<sub>4</sub>:Nd<sup>3+</sup>/NaGdF<sub>4</sub> nanocrystals with efficient near-infrared to near-infrared downconversion photoluminescence for bioimaging applications. *J. ACS Nano* **2012**, *6*, 2969–2977. [[CrossRef](#)] [[PubMed](#)]

22. Ren, W.; Gan, T.; Shan, J.; Gu, Z.; Zhou, L.; Yan, L.; Jin, S.; Yin, W.; Zhao, Y. TWEEN coated NaYF<sub>4</sub>:Yb,Er/NaYF<sub>4</sub> core/shell upconversion nanoparticles for bioimaging and drug delivery. *J. RSC Adv.* **2012**, *2*, 7037–7041. [[CrossRef](#)]
23. Boyer, J.-C.; Gagnon, J.; Cuccia, L.A.; Capobianco, J.A. Synthesis, characterization, and spectroscopy of NaGdF<sub>4</sub>:Ce<sup>3+</sup>,Tb<sup>3+</sup>/NaYF<sub>4</sub> Core/Shell nanoparticles. *J. Chem. Mater.* **2007**, *19*, 3358–3360. [[CrossRef](#)]
24. Jin, S.; Zhou, L.; Gu, Z.; Tian, G.; Yan, L.; Ren, W.; Yin, W.; Liu, X.; Zhang, X.; Hu, Z.; et al. A new near infrared photosensitizing nanoplatfrom containing blue-emitting up-conversion nanoparticles and hypocrellin A for photodynamic therapy of cancer cells. *J. Nanoscale* **2013**, *5*, 11910–11918. [[CrossRef](#)] [[PubMed](#)]
25. Lezhnina, M.; Jüstel, T.; Kätker, H.; Wiechert, D.U.; Kynast, U.H. Efficient luminescence from rare-earth fluoride nanoparticles with optically functional Shells. *J. Adv. Funct. Mater.* **2010**, *16*, 935–942. [[CrossRef](#)]
26. Bo, S.H.; Hu, J.; Chen, Z.; Wang, Q.; Xu, G.M.; Liu, X.H.; Zhen, Z. Core-shell LaF<sub>3</sub>: Er,Yb nanocrystal doped sol-gel materials as waveguide amplifiers. *J. Appl. Phys. B* **2009**, *97*, 665. [[CrossRef](#)]
27. Zhou, B.; Tao, L.; Tsang, Y.; Jin, W. Core-shell nanoarchitecture: A strategy to significantly enhance white-light upconversion of lanthanide-doped nanoparticles. *J. Mater. Chem. C* **2013**, *1*, 4313–4318. [[CrossRef](#)]
28. Vetrone, F.; Naccache, R.; Mahalingam, V.; Morgan, C.G.; Capobianco, J.A. Upconverting nanoparticles: The active-core/active-shell approach: A strategy to enhance the up conversion luminescence in lanthanide-doped nanoparticles. *J. Adv. Funct. Mater.* **2010**, *19*, 2924–2929. [[CrossRef](#)]
29. Chen, D.; Yu, Y.; Huang, F.; Lin, H.; Huang, P.; Yang, A.; Wang, Z.; Wang, Y. Lanthanide dopant-induced formation of uniform sub-10 nm active-core/active-shell nanocrystals with near-infrared to near-infrared dual-modal luminescence. *J. Mater. Chem.* **2012**, *22*, 2632–2640. [[CrossRef](#)]
30. Yang, D.; Li, C.; Li, G.; Shang, M.; Kang, X.; Lin, J. Colloidal synthesis and remarkable enhancement of the upconversion luminescence of BaGdF<sub>5</sub>:Yb<sup>3+</sup>/Er<sup>3+</sup> nanoparticles by active-shell modification. *J. Mater. Chem.* **2011**, *21*, 5923–5927. [[CrossRef](#)]
31. Zhang, Y.; Liu, X.; Lang, Y.; Yuan, Z.; Zhao, D.; Qin, G.; Qin, W. Synthesis of ultra-small BaLuF<sub>5</sub>:Yb<sup>3+</sup>,Er<sup>3+</sup>@BaLuF<sub>5</sub>:Yb<sup>3+</sup> active-core-active-shell nanoparticles with enhanced up-conversion and down-conversion luminescence by a layer-by-layer strategy. *J. Mater. Chem. C* **2014**, *3*, 2045–2053. [[CrossRef](#)]
32. Zhai, X.; Liu, S.; Liu, X.; Wang, F.; Zhang, D.; Qin, G.; Qin, W. Sub-10 nm BaYF<sub>5</sub>:Yb<sup>3+</sup>,Er<sup>3+</sup> core-shell nanoparticles with intense 1.53 μm fluorescence for polymer-based waveguide amplifiers. *J. Mater. Chem. C* **2013**, *1*, 1525–1530. [[CrossRef](#)]
33. Lei, L.; Chen, D.; Huang, F.; Yu, Y.; Wang, Y. Syntheses and optical properties of monodisperse BaLnF<sub>5</sub> (Ln = La–Lu, Y) nanocrystals. *J. Alloy. Compd.* **2012**, *540*, 27–31. [[CrossRef](#)]
34. Wang, M.; Liu, J.L.; Zhang, Y.X.; Hou, W.; Wu, X.L.; Xu, S.K. Two-phase solvothermal synthesis of rare-earth doped NaYF<sub>4</sub> upconversion fluorescent nanocrystals. *J. Mater. Lett.* **2009**, *63*, 325–327. [[CrossRef](#)]
35. Sani, E.; Toncelli, A.; Tonelli, M. Effect of Cerium codoping on Er:BaY<sub>2</sub>F<sub>8</sub> crystals. *J. Opt. Express* **2005**, *13*, 8980–8992. [[CrossRef](#)]
36. Shen, S.; Richards, B.; Jha, A. Enhancement in pump inversion efficiency at 980 nm in Er<sup>3+</sup>, Er<sup>3+</sup>/Eu<sup>3+</sup> and Er<sup>3+</sup>/Ce<sup>3+</sup> doped tellurite glass fibers. *J. Opt. Express* **2006**, *14*, 5050–5054. [[CrossRef](#)]
37. Meng, Z.; Yoshimura, T.; Fukue, K.; Higashihat, M.; Nakat, Y.; Okada, T. Large improvement in quantum fluorescence yield of Er<sup>3+</sup>-doped fluorozirconate and fluoroindate glasses by Ce<sup>3+</sup> codoping. *J. Appl. Phys.* **2000**, *88*, 2187–2190. [[CrossRef](#)]
38. Johnson, N.J.J.; Sha, H.; Diao, S.; Chan, E.M.; Dai, H.; Almutairi, A. Direct Evidence for coupled surface and concentration quenching dynamics in lanthanide-doped nanocrystals. *J. Am. Chem. Soc.* **2017**, *139*, 3275–3282. [[CrossRef](#)] [[PubMed](#)]

